Catalysis Science & Technology

ARTICLE

Carbon Dissolution and Segregation in Platinum

Patanachai Janthon,[abcd] Francesc Viñes,*[a] Jakkapan Sirijaraensre,[bc] Jumras Limtrakul[e] and Francesc Illas[a]

Received 00th January 20xx,
Accepted 00th January 20xx

DOI: 10.1039/x0xx00000x

www.rsc.org/chemicalscience

Recent experimental studies evidenced C dissolution in Pt nanoparticles after CH_4 decomposition, and its low temperature seggregation to form surface graphene, highlighting a graphene growth from below, with indications of an easier C transfer in between surface and subsurface regions at Pt grain boundaries, alhtough the ultimate atomistic mechanism remained unclear. A plausible explanation is provided here by exploring and comparing C incorporation on Ni, Pd, and Pt (111) surfaces by density functional (DF) calculations on slabs models at a low coverage regime, evaluating energetic stability and subsurface sinking kinetic feasiblity. Four DF functionals have been used, avoiding possible biased results. All show that C atoms occupy octahedral subsurface sites (*oss*) in Ni(111), with high sinking energy barriers of 80-90 kJ mol^{-1}, whereas both *oss* and tetrahedral subsurface sites (*tss*) can be occupied on Pd(111), with low sinking energy barriers of 20-50 kJ mol^{-1} . The *oss* sites are strongly disfavoured on Pt(111), whereas *tss* sites are found to be isoenergetic to surface sites, with low subsurface sinking energy barriers of 27-41 kJ mol^{-1}. Calculations on Pt_{79} and Pt_{140} nanoparticle models reveal how *tss* sites are more stabilized at low-coordinated sites, where subsurface sinking energy barriers drop to values of ~17 kJ mol^{-1}. Results explain experimentally observed C dissolution and segregation in Pt systems, more favoured at grain boundarie, as well at the growth from below and formation of double layers. Present results as well open a gate for profiting of small quantities of C placed at the subsurface region to tune the surface catalytic activity of Pt nanoparticle based catalysts.

1. Introduction

The interplay of Carbon and Platinum is paramount in many scientific and technological fields. For instance, Pt nanoparticles synthesized over high surface area, microporous carbon based materials are nowadays widespread used as oxygen reduction reaction (ORR) catalysts in fuel cell technologies.[1] As far as carbon-based nanotechnologies are concerned, Pt single crystal grains have been recently proposed as a template for the controlled graphene tessellation on their surface.[2] However, in heterogeneous catalysis, Carbon is also longstanding regarded as a catalyst poison. Coke, *e.g.* graphitic carbon, generated in the course of a surface catalysed reaction involving organic moieties, is deposited over the metal catalyst surface, blocking the active sites and so severely decimating its performance.[3]

Catalyst deactivation is therefore an undesired yet regretfully common phenomenon, with a high, negative impact in chemical industry. Because of this with many research endeavours are addressed at its mitigation, even to the point of prevention, including the set up of poison[4] and sinter resistant[5] catalysts, as well as catalyst regeneration procedures.[3] However, recent studies have shown that low contents of some catalyst surface poisons are actually beneficial, allowing for the selective isolation of intermediates and final products with a given desirable stereochemistry.[6,7]

This poison-to-promoter role change seems to be case for C_1 atomic species on Pd catalysts employed for hydrocarbon dehydrogenation processes,[8] where the other group X transition metals Ni and Pt are employed as catalysts as well.[9-11] Indeed, a higher performance has been found to be connected to the existence of subsurface C species at hydrocarbon reaction working conditions, with theoretical simulations backing up the experimental determination of carbon residues, which, in the form of either substitutional or interstitial impurities, affect the catalyst selectivity.[12,13]

Subsurface chemistry has been unveiled then as a determinant factor in diverse cutting-edge scientific areas, from the higher reactivity of interstitial C compared to surface C,[14] to the graphene formation and healing by C segregation from Ni_3C.[15,16] High C chemical potentials and moderate or high working temperatures prompt the subsurface sinking of as generated C atoms.[7,17,18] Furthermore, the existence of subsurface C species, which locally distort the surface metal

[a] *Departament de Ciència de Materials i Química Física & Institut de Química Teòrica i Computacional (IQTCUB), Universitat de Barcelona, c/ Martí i Franquès 1, Barcelona 08028, Spain.*
[b] *Department of Chemistry, Faculty of Science, Kasetsart University, Bangkok 10900, Thailand.*
[c] *Center for Advanced Studies in Nanotechnology for Chemical, Food and agricultural Studies, KU Institute for Advanced Studies, Kasetsart University, Bangkok 10900, Thailand.*
[d] *Faculty of Science, Chandrakasem Rajabhat University, Bangkok 10900, Thailand.*
[e] *Department of Materials Science and Engineering, School of Molecular Science and Engineering, Vidyasirimedhi Institute of Science and Technology, Rayong 21210, Thailand.*

geometrical and electronic structure, may favour the incorporation of other moieties, as found to be the case for H in Pd nanoparticles,[19] eventually allowing, by indirect control of the amount of subsurface H, for critically speeding up or slowing down the on-going surface hydrogenation reaction catalysed on Pd nanoparticles.[20]

However, despite being of the same group X, subsurface C species in Pt have been historically disregarded, despite of the experimental evidence of their existence. C impurities are long known to segregate from bulk during Pt single crystal preparation.[21] This has been recently profited to synthesize surface graphene from C dissolved in Pt nanocrystallites, involving methane (CH_4) chemical vapour deposition, its surface full dehydrogenation and C atomic dissolution at high temperatures, followed by a low temperature C segregation.[2,22,23] These experiments provided compelling evidence of C dissolution and a graphene synthesis mechanism from below, providing a response to a longstanding argument about graphene formation from surface aggregation or subsurface segregation.[22] Aside, C absorption/segregation was found to be more facile at Pt grain boundaries.

Therefore, tuning the working conditions allowing for C concentration control as well as of the balance between deposition, and absorption and desorption rates permit to tailor the formation of a continuous graphene layer, few-layer graphene, up to graphite nanocrystallites. This seems to be a key also for the appearance of islands of C impurities beneath the as-formed graphene sheet, misaligned with respect to the graphene layer, known also to form from below. These resemble the so-known double layer model proposed for graphene flakes on Pt(111) surface, also summoned long ago to explain the separation of the carbon layer, now known as graphene, from it.[24,25]

The double layer model has been backed up by theoretical simulations based density functional (DF) theory.[26] However, the crucial question of how could C atoms slide into the graphene/Pt interface remained open. Experimentally, C solubility in Pt at 1000 ºC is 1.14 at. %,[27] similar to that of Ni (1.26 at. %),[28] and actually both molten Pd and Pt feature a similar solubility for C.[27] So, the growth from below appears as an appealing simple explanation for it.

However, this possibility has never been validated from the theoretical point of view. Indeed octahedral subsurface (oss) site occupation has been found to be endothermic by ~60 kJ mol^{-1}, according to DF calculations on Pt(111) surface slab model.[26] In addition the lower Pt ductility compared to Ni and Pd, as a result from a stronger Pt metal bonding, implies a cost for structural relaxation nine times larger than Pd or Ni, and so this factor plays against C incorporation, despite the higher melting Pt is appealing for graphene synthesis control.[2] All in all, C dissolution in Pt remains an open question where the diverse puzzle pieces do not fit together.[29]

To provide an unbiased answer to this and to fill the necessary lack of mechanistic detail on C dissolution and segregation processes on Pt systems, we carried out a full state-of-the-art DF of them on Ni, Pd, and Pt surfaces, thus evaluating the stability of all subsurface and surface species, as well as the subsurface sinking energy barriers. Through this systematic study a complete picture of the energetics and kinetics of subsurface C moieties formation is gained. The obtained results at different levels of theory show that while C atoms prefer to occupy *oss* sites in Ni, they occupy both *oss* and tetrahedral subsurface sites (*tss*) on Pd, and, more importantly, they also can occupy *tss* sites in Pt. For Pt, *tss* stability is further strengthened at undercoordinated sites, as shown on Pt_{79} and Pt_{140} nanoparticles, accompanied by a subsurface sinking energy barrier reduction. Present results strong support the existence of subsurface C in Pt systems and explain to the above-commented graphene segregation on Pt surfaces, the double layer model, and the preferential absorption on Pt grain boundaries. Control of subsurface C can be envisaged as a way to tune the surface Pt catalytic activity, specially at low coordinated sites, thus contributing into the rational design of tailored Pt-based heterogeneous catalysts.

2. Computational details

The DF calculations have been carried out using the VASP code exploding periodic boundary conditions.[30] Geometries and total energies reported in the following were optimized using four different exchange-correlation (xc) functionals, including the Perdew-Wang (PW91),[31] the Perdew-Burke-Ernzerhof (PBE),[32] and the revised Perdew-Burke-Ernzerhof (RPBE)[33] functionals within the generalized gradient approximation (GGA), and the Vosko-Wilk-Nusair (VWN)[34] as a representative of the local density approximation (LDA) family. The Ceperley-Alder (CA) LDA type[35] was not used since provides essentially same results as VWN for transition metals. [36,37] The underlying reason to explore many xc functionals is to better assure an unbiased outcome, since *e.g.* VWN and CA are known to overestimate interatomic interactions, whereas RPBE for instance is known to underestimate them.[36]

Valence electrons density was expanded in a plane wave basis set with a 415 eV cutoff for the kinetic energy and the projector augmented wave method was used to describe the interactions between core and valence electrons.[38] Spin polarized calculations were carried out for magnetic Ni, and non-spin polarized for nonmagnetic Pd and Pt metals. A 54 metal atoms (3×3) supercell slab was used to model the (111) surface of the three metals. The slab models contained six atomic layers with nine atoms per layer. The three bottom layers of the slab were kept fixed at the optimized yet bulk-terminated geometry, while the other three upper layers were allowed to further relax during geometry optimization, together with the adsorbed/absorbed carbon atom. The reciprocal space was sampled with 6×6×1 **Γ**-centered **k**-point grid and calculations were performed using a Gaussian smearing of 0.2 eV energy width to speed up convergence, yet final energies where extrapolated to 0 K (no smearing).

In addition, Pt_{79} and Pt_{140} nanoparticle models were also used allowing a comparison among extended regular surfaces and low coordinated sites at Pt nanoparticle grain boundaries. For a depiction of Pt_{79} and Pt_{140} cuboctahedral nanoparticles we refer to the literature.[26,39] Briefly, Pt nanoparticles have been calculated by placing them in a cubic box imposing a

minimum distance of 10 Å in between translationally repeated nanoparticles and considering the Γ point only. The same procedure was used to compute the energy of the isolated C atom, hence an asymmetric box of 9×10×11 Å has been used to assure the correct orbital occupancy featuring a triplet state. In all cases, geometry optimizations were performed until all forces acting on relaxed atoms became less than 0.03 eV Å^{-1}.

Several positions are possible for the adsorption or absorption of C atoms on the *fcc* (111) metal surfaces. Herein we sampled three adsorption and three absorption sites, shown in Fig. 1: Top site and *fcc* and *hcp* three-fold hollow sites for the adsorption, and *oss* and two types of *tss* for subsurface C. Note that *oss* is located below an *fcc* surface site, whereas *tss* is located below a surface *hcp* hollow site. The *tss'* site is located just below a surface top metal atom. Given the employed supercell, calculations imply a C (sub)surface coverage of $^1/_9$ monolayer (ML).

The activation energy barriers associated to a surface-to-subsurface diffusion were determined by scanning the potential energy profile along the line that connects the local minima of the surface and subsurface impurity atoms. Thus estimations of Transition States (TSs) were searched in a point-wise fashion along the path connecting adsorption and absorption configurations, where height of the carbon atom, defined with respect to the most distant frozen metal layer, was fixed, whereas all other degrees of freedom were allowed to fully relax. Subsequently, each of these approximate TSs was refined allowing C displacement along surface/facet direction by a quasi-Newton method, until forces acting on atoms were below 0.03 eV Å^{-1}. The resulting TS structures have been characterized by vibrational frequency analysis, certifying their saddle point nature.

We define the calculated adsorption/absorption energies as;

$$E_{ads/abs} = -E_{C/metal} + (E_C + E_{metal}) \qquad (1)$$

where $E_{C/metal}$ is the total energy of the metal model with the C atom either adsorbed or absorbed, E_C is the energy of an isolated carbon atom, and E_{metal} is the energy of the optimized clean substrate: Ni, Pd, and Pt (111) surface slab models, or Pt_{79} or Pt_{140} nanoparticles. With this definition, stable adsorption/absorption corresponds to positive $E_{ads/abs}$ values.

3. Results

3.1. C adsorption/absorption on/in metal surfaces

Let us first start with the energetic stability of C atoms on Ni, Pd, and Pt (111) surfaces, as well as in their first subsurface layer. Adsorption and absorption energies are listed in Table 1, and plotted in Fig. 2. From the obtained results some general features are clearly evident. First, both PW91 and PBE xc functionals provide essentially same results, with discrepancies of, at most, 6 kJ mol^{-1}, thus well within standard DF accuracy of ~10 kJ mol^{-1}, and in accordance, for instance, the very similar performance of PBE and PW91 in transition metal bulk properties.[36] Along this line, VWN results always depict stronger adsorption/absorption situations, whereas the opposite applies for RPBE, again in line with previous results on transition metal bulks,[36] yet one clearly notices that, aside from the bonding strengthening/weakening, relative positions of ad/absorption sites are consistently predicted, and so, any of the tested xc functionals is depicting the very same chemical situation.

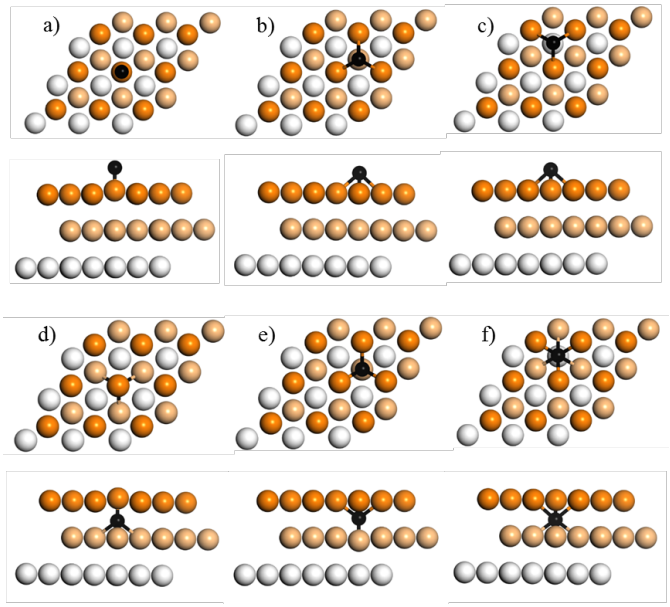

Fig. 1 Top (top) and side (bottom) views of the employed models for C moieties on/in the (111) *fcc* metal surface; a) *top*, b) *hcp*, c) *fcc*, d) *tss'*, e) *tss*, and f) *oss* sites. C atoms are shown as black spheres. Metal surface layer is depicted by dark orange spheres, whereas first and second subsurface layers by light-orange and white spheres, respectively.

Moreover, in all cases, surface adsorption top site is markedly less stable than *hcp* or *fcc* hollows —by more than 210 kJ mol^{-1} in the best case— and so has not been further considered as a possible site for adsorbed C atoms. Last but not least, notice that adsorption and absorption energies feature values above 500 kJ mol^{-1} whatever the metal or the employed xc functional, thus showing a highly strong interaction, in agreement with previous DF studies.[26,40,41]

Focusing the attention, adsorption energies for C on Ni(111) surface are of the same order of magnitude than low-coverage reported values reported in the literature ranging 640-700 kJ mol^{-1}, as obtained at PW91 or PBE levels,[40-44] with differences stemming out probably from slight differences in **k**-points sets, basis sets, and employed supercells sizes. It is noteworthy that present results reveal a slight preference for *hcp* site compared to *fcc*, by ~4 kJ mol^{-1}, in excellent agreement with earlier calculations.[40,42,44] Last, the higher stability of subsurface C the *oss* site below the Ni(111) surface is out of doubt, with previous studies stating an absorption energy above 700 kJ mol^{-1} at PW91 and PBE levels[40,42,44] —here 718 and 715 kJ mol^{-1}, respectively— being surface C atom at *fcc* further stabilized by 50-60 kJ mol^{-1} when sinking subsurface to occupy *oss* sites, according to the literature, and

Table 1 Adsorption (E_{ads}) and absorption (E_{abs}) energies of C atom on Ni, Pd, and Pt (111) surfaces, obtained using different exchange-correlation (xc) functionals; VWN, PW91, PBE, and RPBE. All values are given in kJ mol^{-1}.

xc	E_{ads} / E_{abs}	Ni(111)	Pd(111)	Pt(111)
VWN	*top / tss'*	512 / 725	492 / 772	538 / 736
	hcp / tss	769 / 704	777 / 792	783 / 780
	fcc / oss	764 / 836	775 / 851	796 / 747
PW91	*top / tss'*	435 / 615	420 / 682	477 / 654
	hcp / tss	666 / 607	681 / 703	692 / 697
	fcc / oss	662 / 718	680 / 743	706 / 648
PBE	*top / tss'*	434 / 613	421 / 683	478 / 654
	hcp / tss	663 / 601	682 / 704	694 / 697
	fcc / oss	659 / 715	681 / 746	708 / 650
RPBE	*top / tss'*	403 / 578	392 / 651	454 / 623
	hcp / tss	621 / 561	647 / 671	660 / 666
	fcc / oss	619 / 669	646 / 707	674 / 614

presently being 56 kJ mol^{-1} both at PW91 and PBE levels. The results are similar as well for VWN and RPBE estimates.

This situation changes, however, when considering Pd instead of Ni. Here it is remarkable how adsorption energy on *hcp* and *fcc* sites slightly increases with respect Ni, by 10-20 kJ mol^{-1}, at any of the DF levels employed in the present work. However, the largest change occurs subsurface. Both *tss* and *oss* sites are more stable than the respective surface *hcp* and *fcc* sites. Indeed, even *tss'* is competitive to surface sites, being considered isoenergetic —differences in interaction strength below 6 kJ mol^{-1}— and actually in fully agreement with previous calculations at RPBE level by Nykänen *et al.*[45] Indeed, *oss* sites are much more stable than corresponding surface *fcc* sites, by 60-76 kJ mol^{-1}, depending on the xc functional, and so, more stabilized than on Ni. This fact aligns with an experimentally observed Pd-C interphase,[46] and correlates with the larger Pd interatomic distance compared to Ni, by more than 25 pm;[36] the larger interatomic distance translates into more spacious subsurface sites, where C atoms better accommodate.

As happened with Ni(111) surface, present results for Pd(111) fully agree with the bond strengths and the slight hcp preferential adsorption —by 1-4 kJ mol^{-1}— observed by previous estimations at low coverage as obtained at VWN, PW91, and RPBE levels,[13,19,45] and actually as well to estimates, obtained *via* a computing strategy combining PW91 or RPBE energy values on as-obtained VWN geometries.[19,41] However this strategy may lead to strange behaviours; for instance, the preference of *tss* over *hcp*, here estimated to be 22 and 24 kJ mol^{-1} at PW91 and RPBE xc levels, reduces to 6 and 5 kJ mol^{-1} when carrying out calculations on VWN geometries, easily understood by a significant decrease of the Pd-Pd distance at VWN compared to PW91 and RPBE levels, by *circa* 7 and 9 pm, respectively.[36]

So, the smallest stabilization relates to an artificial tightening of the *tss* room which indeed originates from the larger self interaction error in LDA type functionals. Moreover, self-consistent VWN subsurface stabilization values agree within 3 kJ mol^{-1} with respect those in the literature,[19] and solely vary by at much 6 and 10 kJ mol^{-1} with those earlier obtained at PW91[13,47] and RPBE[45] levels. Solely a slight disagreement is found for *tss* stabilization over *hcp* at PW91 with the work of Kozlov *et al.*,[13] where an isoenergetic situation was found, whereas here a sensible stabilization by 22 kJ mol^{-1} is found. Probably slab model, **k**-points density, basis set quality, and the employed supercell are key factors at the origin of such a discrepancy.

A case apart is Pt(111): Previous RPBE calculations revealed a preference of *fcc* site over *hcp* by ~14 kJ mol^{-1}, value reproduced here with any of the explored xc functionals.[26] The change on the adsorption site preference is alleged to be due to a subsurface electron density steric repulsion. Aside, following the same Ni→Pd trend, E_{ads} values for *hcp* and *fcc* sites are 10-30 kJ mol^{-1} larger than for Pd, and so, adsorption strength along the group nicely correlates with *d*-band centre and/or upper *d*-band edge electronic descriptors.[48] In addition, adsorption strengths are perfectly in line with those obtained by Michaelides and Hu using the PW91 functional.[49]

The other remarkable point is that *oss* is sensibly destabilized with respect *fcc* surface site, as clearly observed in Fig. 2. The destabilization is large, by 50-60 kJ mol^{-1}, and in perfect agreement with previous estimates at RPBE level.[26] Clearly, the longer Pt-Pt distance is not translated in a better accommodation of C in the larger *oss* sites, and actually is rather detrimental. Indeed, an optimum *oss* environment for C seems to be achieved using Pd, but on Pt this slightly larger bond length appears to be excessive, and the interaction gets weakened. Quite surprisingly, C at subsurface *tss* site in Pt(111) appears to be strengthened. Here, at PW91, PBE, and RPBE xc levels, *tss* is slightly more stable than the above surface *hcp* site, by 3-6 kJ mol^{-1}, although less stable by 3 kJ mol^{-1} at VWN level. Indeed, it appears that space is playing a key role in subsurface stabilization, which accords with VWN results, where Pt-Pt distances are sensibly shorter, and so *tss* is less stabilized. The most surprising result here is that, for the first time, *tss* subsurface site in Pt(111) is found to be at least competitive to any of the surface *fcc* or *hcp* sites for C atoms. However, so far only thermodynamic aspects have been

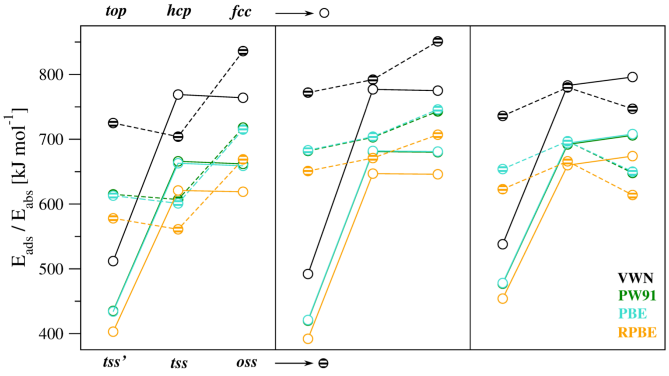

Fig. 2 Adsorption (E_{ads}) and absorption (E_{abs}) energies of C atom on Ni (left), Pd (middle), and Pt (right) (111) surfaces, obtained using different xc functionals; VWN, PW91, PBE, RPBE. All values are given in kJ mol^{-1}.

contemplated. In the next section we inspect whether kinetic aspects would inhibit or favour such a subsurface occupancy.

3.2. C subsurface sinking

In this section we investigate the feasibility of C subsurface migration by estimating the subsurface sinking process activation energy. To this end TSs have been located following the *hcp*↔*tss* and *fcc*↔*oss* paths and appropriately characterized. Forth and back activation energies are encompassed in Table 2, and subsurface diffusion profiles in Fig. 3. From the results it is clear that subsurface diffusion profiles for any path are generally equivalent when calculated with any of the employed functionals. Actually, TSs heights for critical steps may differ by up to ~15 kJ mol^{-1}, but clearly this is biased by the relative position of initial and final states, as expected from the Brønsted-Evans-Polanyi (BEP) relationships on transition metals,[50,51] and the fact that these are actually not heavily influenced by the employed level of theory.[52] All that said, it is to highlight that on Ni(111) the C atoms are thermodynamically driven to occupy *oss* sites, yet a high barrier of 80-90 kJ mol^{-1} is needed to be overcome.

The relatively high energy barriers are in line with the experimental observation of C subsurface diffusion at temperatures above 700 K.[53] The barrier height would actually fit with the reported value of Massaro and Petersen[54] of 84 kJ mol^{-1}, yet actually much higher barriers are found in the literature, ranging 167-193 kJ mol^{-1}.[53,55] It is worth to mention that previous computational studies on models implying a coverage of ¼ ML carried out with the PBE functional show subsurface diffusion barriers towards *oss* site of 177-185 kJ mol^{-1}, and hence, close to experiments.[12,40] However, Cinquini *et al*.[42] clearly showed that such high barriers are an artefact of using an exceedingly small *p*(2×2) supercell.

In fact, the lateral displacement of surface Ni atoms in the TS implies a strong slab tension, which raises the TS energy. Using the PW91 functional, these authors estimated an energy barrier using a *p*(2×2) supercell of 164 kJ mol^{-1}, and a value of 71 kJ mol^{-1} using a *p*(3×3) supercell, which nicely correlates with present results using the same cell dimension. The higher experimental energy barriers are probably due to the posterior bulk diffusion of the subsurface C atoms, estimated to be 156-166 kJ mol^{-1} at PW91 level,[42,56] which would act as a rate limiting step.

Table 2 Subsurface (E_{sub}) and surface (E_{sur}) migration activation energy barriers for a C atom on Ni, Pd, and Pt (111) surfaces, obtained using different exchange-correlation functionals; VWN, PW91, PBE, and RPBE. All values are given in kJ mol^{-1}.

xc	E_{sub} / E_{sur}	Ni(111)	Pd(111)	Pt(111)
VWN	*hcp*↔*tss*	78 / 14	33 / 48	41 / 38
	fcc↔*oss*	90 / 162	49 / 125	104 / 55
PW91	*hcp*↔*tss*	66 / 7	22 / 45	29 / 34
	fcc↔*oss*	79 / 135	39 / 102	96 / 38
PBE	*hcp*↔*tss*	69 / 8	23 / 45	31 / 34
	fcc↔*oss*	81 / 137	40 / 104	97 / 40
RPBE	*hcp*↔*tss*	80 / 19	20 / 44	27 / 33
	fcc↔*oss*	94 / 144	37 / 98	96 / 36

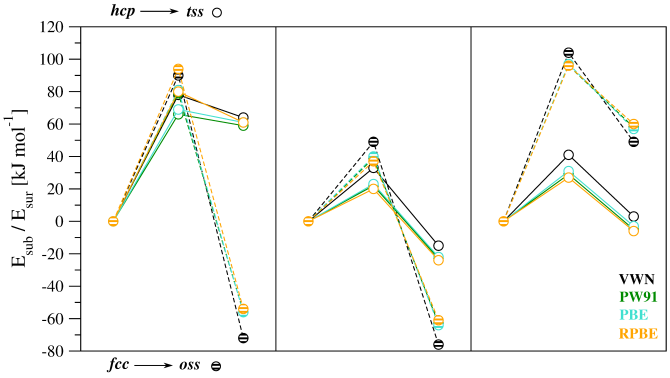

Fig. 3 Subsurface (E_{sub}) and surface (E_{sur}) C diffusion energy profiles for the *hcp*↔*tss* and *fcc*↔*oss* paths on Ni (left), Pd (middle), and Pt (right) (111) surfaces, obtained using different xc functionals; VWN, PW91, PBE, and RPBE. For comparative purposes, all *fcc* and *hcp* adsorption energies are equalled in energy and used as zero energy reference. All values are given in kJ mol^{-1}.

When comparing Ni to Pd, one observes in Pd that both *oss* and *tss* sites can be kinetically occupied, since subsurface diffusion energy barriers are similar in height. Indeed, the *tss* sites, despite being less stable than *oss*, display lower energy barriers compared to barriers towards *oss* by ~16 kJ mol^{-1}, in full agreement with previous PW91 estimations on VWN structures.[41] Note that, whatever the subsurface site, C incorporation implies overcoming energy barriers of 20-50 kJ mol^{-1}. This signifies that C penetration is easier than C adatom surface diffusion, which has an energy barrier of almost 70 kJ mol^{-1} as obtained at PW91 level,[13] and being also smaller than the dehydrogenation barriers in C atom formation from methane[57] or ethylene,[58] being as high as 125 and 154 kJ mol^{-1} as obtained at RPBE and PW91 levels, respectively.

So, whenever C atoms are on the Pd(111) surface, they sink subsurface, being neither their formation nor their surface diffusion the limiting step towards the formation of a Pd-C phase. The larger malleability of Pd compared to Ni and the larger intermetallic distances are both at the origin of the increased subsurface stability and kinetic feasibility for subsurface C species. Note that this correlates with a smaller experimentally determined subsurface diffusion energy barrier of 107-155 kJ mol^{-1}.[59,60] Present values fit with energy barriers for *oss* occupation of 53 kJ mol^{-1} as obtained at PW91 level by Gracia *et al*.,[47] and also values of 53 and 48 kJ mol^{-1} for *oss* and *tss* occupation by Nykänen *et al*. obtained at RPBE level.[45] In this last work it was shown how diffusion towards bulk implies larger barriers in the range of 121-177 kJ mol^{-1}, thus fitting the above commented experimental values, and backing up a bulk diffusion rate limiting step, rather than the actual subsurface diffusion.

The case of Pt(111) seems just the contrary as to Ni(111). Because of the above commented instability of C at *oss* sites, the energy barriers towards it are rather large, in the 95-105 kJ mol^{-1} range, whereas the surface emerging ones are sensibly small, in between 35-55 kJ mol^{-1}. So, occupancy of *oss* sites is hindered both because of thermodynamic and kinetic reasons. Surprisingly, a completely different situation is found for the

tss sites. Thermodynamically, they are of similar energy to *hcp* surface sites, and the subsurface energy barriers —and so the surface emerging ones— are relatively small as in the Pd case, here of 25-45 kJ mol^{-1} height. This implies a possible occupancy of *tss* sites at room temperature, and undoubtedly at methane or ethylene dehydrogenation working conditions,[2,22,23] where rate limiting steps have been found to be of 120 kJ mol^{-1} for methane, as obtained from RPBE,[57,61] and 143 kJ mol^{-1} from ethylene as obtained from PW91 DF calculations.[58] As happened with Pd, the surface diffusion among *fcc* and *hcp* sites was previously estimated on Pt(111) to be of 70-90 kJ mol^{-1} at RPBE level, and so, diffusion would be no limitation in C subsurface occupancy of *tss* sites.

Thus, so far, we have shown how C atoms can entrench on Pt(111) surfaces occupying subsurface *tss* sites even at low temperatures. Apparently, the *hcp*↔*tss* route, displaying low energy barriers, is the gate both for the C dissolution and segregation processes, switched on/off by the C chemical potential at the surface and subsurface regions. Moreover, the stability of C atoms in tetrahedral interstitial sites inside Pt seems to play a major role in C incorporation on Pt based composites. The above commented experimental similarity between Pd and Pt concerning C affinity,[27] and the carbon dissolution and segregation phenomena, including the double layer model, is so now understood.[2,21-25]

At this point, one may wonder, given the above stated similarity in between Pd and Pt, whether subsurface C could be further stabilized at Pt low-coordinated sites, as found for Pd. In the latter, subsurface diffusion has been found to be essentially barrierless at edges and corners of Pd nanoparticles boundaries,[41] driven by a further accommodation in such sites. This links to a significant low energy cost relaxation to accommodate subsurface C on these sites, and so supporting previous experimental statements suggesting existence of carbonaceous deposits at edges between (111) facets of Pd nanoparticles.[62]

Such a large reduction in subsurface sinking energy barriers has also been found on Pd(211) steps according to the RPBE simulations by Nykänen *et al*.[45] Furthermore, the existence of such subsurface C atoms in Pd nanoparticles has been found to promote H incorporation both thermodynamically and kinetically.[19,20,63] Indeed, Babar and coworkers suggested that some sites of Pt nanoclusters may become more active once C is adsorbed, and eventually stronger bind H.[64] The question mark here is whether such subsurface C atoms at low-coordinated sites in Pt nanoparticles would be further stabilized, further backing up their usage to tune, for instance, on-going surface catalysed (de)hydrogenation or oxygen reduction reactions. This is further addressed in the following section.

3.3. Subsurface C at low-coordinated sites

In order to ascertain whether C atoms are further stabilized at low coordinated sites of Pt nanoparticles, we employ two nanoparticles: Pt_{79} and Pt_{140}, which are within the regime of properties scalable to bulk.[65] For details of such cuboctahedral nanoparticles we refer to previous literature.[26,57] Since all the tested xc functionals provide very similar results, we restricted these more time consuming calculations to the use of the PBE functional. Furthermore, from Fig. 3, it is clear that *tss* sites are actually favoured towards C occupation, and so, only *hcp* and *tss* sites have been sampled on Pt_{79} and Pt_{140} models, as shown in Fig. 4.

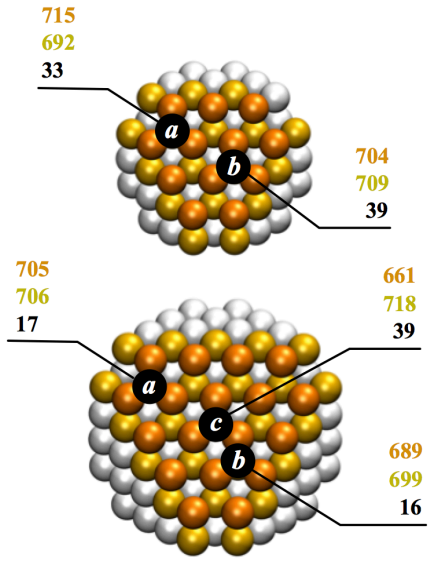

Fig. 4 Adsorption (E_{ads}, in dark orange) and subsurface absorption (E_{abs}, in light orange) energies, in kJ mol^{-1}, on surface *hcp* and subsurface *tss* sites at corner (*a*), edges (*b*), or central (*c*) sites of (111) facets of Pt_{79} and Pt_{140} nanoparticle models, as obtained at PBE level. C diffusion energy barrier for the *hcp*→*tss* path on each site is shown in black.

Results reveal that on Pt_{79} the C atoms adsorbed on *hcp* hollows at (111) facet corner and edge sites, named *a* and *b*, respectively, attach with a somewhat enhanced adsorption energy; compare values of 715 and 704 kJ mol^{-1} to the equivalent value of 694 kJ mol^{-1} on the Pt(111) model. Notice that such enhancement can have different origins; on one side the Pt_{79} nanoparticle is at the fringe limit of the scalable regime, and so, such adsorption energy values could be simply related to this particular size & shape. Moreover, the nm size implies a quantum confinement, which would enhance the very chemical activity, and even more, site coordination is known to play a key role in modulating the adsorption energy.[66] All that considered, C adsorption seems to be slightly improved at corners and edges of the Pt_{79} nanoparticle. However, this does not necessarily apply to *tss* sites. Here, C at *tss* just below corner site of Pt_{79} is slightly destabilized by 5 kJ mol^{-1} compared to *tss* in Pt(111), whereas C at *tss* below the edge site is stabilized 12 kJ mol^{-1}. Note that in such subsurface sites the lower coordination and material flexibility goes for a larger C stabilization, although the reduced Pt interatomic distances imply smaller *tss* cavity, and so has an opposite effect. In any of the explored sites the subsurface diffusion implies a barrier of 30-40 kJ mol^{-1}, and so, very similar to the value of 31 kJ mol^{-1} obtained on the Pt(111) slab model, which seems to indicate that both factors are compensated.

The situation appears to change when moving to a larger nanoparticle, and so, a more representative model for Pt

nanoparticle grain boundary regions. Pt_{140} is well within the size region of properties scalable to bulk, and here quantum size effects are attenuated compared to Pt_{79}. This explains how adsorption on C atom on *hcp* sites of the (111) facet implies a bonding strength smaller than those sampled cases on Pt_{79}. Compare for instance how E_{ads} values in Fig. 4 drop by 10 and 15 kJ mol^{-1} in *a* and *b* sites. Note as well that adsorption energy on the *hcp* site at the centre of the (111) facet, the so-called *c* site, implies a reduced adsorption energy of 661 kJ mol^{-1}, 33 kJ mol^{-1} less than the obtained value on the Pt(111) slab model. Given the shorter Pt-Pt distances, the steric repulsion of the subsurface Pt atom seems to play a determinant role in such a destabilization.

However, surface flexibility due to higher degrees of freedom are the response for the subsurface stabilization, and also the larger Pt-Pt distances compared to Pt_{79}, lengthened in average by ~0.5 pm, from 274.0 pm in Pt_{79} to 274.4 in Pt_{140}. In this rather large Pt nanoparticle, subsurface C atoms at any site are more stable than at surface sites, contrarily with what was found on corner site for Pt_{79}. Moreover, the subsurface sinking site at the central site of the (111) facet features an energy barrier of 33 kJ mol^{-1}, thus in line with the value of 31 kJ mol^{-1} obtained on the Pt(111) slab model. However, the larger stabilization by 57 kJ mol^{-1} relative to Pt(111) would indicate a longer residence of this subsurface C atom. Furthermore, as happened on Pd nanoparticles,[41] the subsurface sinking at the corner and edge low-coordinated sites features a sensibly reduced energy barrier of ~17 kJ mol^{-1}, thus going for a subsurface C presence at defects of Pt nanoparticle systems and Pt steps even at low temperatures, and a much easier transfer for C atoms from and towards the subsurface region. This result is in perfect agreement with the observed preference of C to absorb on Pt at grain boundaries, as well as the growth from them.[22]

In that sense, a similar mechanism for H ad/absorption modulation *via* subsurface C, as observed on Pd nanoparticle systems, seems plausible, and offers a simple yet intuitive explanation to the experimental observations of Babar and coworkers.[64] The effect of subsurface C in Pt may have also as well implications on oxygen reduction reactions; to name few, defective Pt(111) facets have been theoretically proposed as a way of improving Pt catalysts for the ORR,[66] and, inevitably, C impurities, when present, would reside subsurface of such defective higher active sites, modifying the surface on-going reaction. Moreover, oxygen subsurface impurities are known to be generated in Pt based catalysts during ORR,[67] including Pt@Pd and Pt@Ni systems,[68,69] and argued to play a determinant role in a successful operation by destabilizing surface hydroxyls due to electrostatic repulsion, even though subsurface O formation is a highly endothermic process, only achieved with a high surface chemical potential.[70] Clearly subsurface C, also negatively charged, could be easier formed with forecasted similar effect on surface processes.

4. Conclusions

Carbon is a usual support for Pt nanoparticle catalysts, yet carbon deposits formed in Pt surface poison the nanoparticle performance. Subsurface C present in other group X metals Ni and Pd are known to be a critical factor in graphene segregation processes, but also, in low contents, improving the surface catalytic activity either being more active than surface C moieties, by desirably tuning the surface catalytic activity, or by enhancing the metal incorporation of other reacting species, such as found for H on Pd nanoparticles. Recently. strong experimental evidence of C dissolution in Pt systems has been found,[2] confirming a graphene formation by C segregation from below, although the detailed atomistic mechanism remained unveiled.

Here all the experimental observations are explained *via* a thorough density functional study. We fully explored atomic C incorporation on Ni, Pd, and Pt (111) surface systems on proper supercell slab models, allowing for determining the relative stability of C atoms at surface and subsurface sites at a low coverage regime, while estimated subsurface sinking energy barriers permit one determining the kinetic role on the process and the working conditions at which such processes are feasible.

The results have been obtained using four different exchange-correlation functionals to avoid possible bias on the results obtained from a particular choice, yet all the employed methodologies deliver the same picture: C atoms are thermodynamically driven to occupy octahedral subsurface sites (oss) in Ni(111), despite of featuring high energy barriers of 80-90 kJ mol^{-1}, and so, these would only be occupied at high temperature working conditions, as experimentally observed. Both *oss* and tetrahedral subsurface sites (tss) would be occupied on Pd(111) but at lower temperatures, as energy barriers for subsurface occupancy are in the 20-50 kJ mol^{-1} range. Last but not least, according to present calculations, *oss* sites are hindered on Pt(111), being 50-60 kJ mol^{-1} less stable than immediately superior *fcc* surface sites, whereas *tss* sites are found to be essentially isoenergetic to immediately superior surface *hcp* sites. Thus, *tss* subsurface sites are probably sampled on Pt systems, given that subsurface sinking energy barriers are low, of 27-41 kJ mol^{-1} height, explaining the similar C dissolution capability of Pt compared to Pd, and the low temperature segregation to form surface graphene.

The analysis of structural effects shows how the size of subsurface space sites is related to the interatomic metal distances and the relaxation upon subsurface occupancy. This is at the origin of the stabilization in *tss* and *oss* sites. Last but not least, such *tss* occupancy has been further found on Pt_{79} and Pt_{140} nanoparticles, representative of larger Pt nanoparticle systems. Here the smaller room due to nanoparticle contraction is counteracted by an enhanced chemical activity. Compared to Pt(111) extended surfaces or terraces, C at *tss* sites near low-coordinated sites of the nm sized Pt_{140} particle are slightly more stabilized but, more importantly, subsurface energy sinking drops to values of ~17 kJ mol^{-1}, implying a low-temperature occupancy of *tss* sites by C, in a similar fashion to what was observed on similar metal Pd, and explaining the observation of a stronger absorption and segregation of C atoms at Pt grain boundary regions. Present results reveal the possible modulating role of C

impurities at Pt low-coordinated sites on the on-going surface catalysed processes.

Acknowledgements

This work was supported by Spanish *MINECO* grant CTQ2015-64618-R and, in part, by *Generalitat de Catalunya* grants (2014SGR97 and XRQTC). P.J. would like to thank the Office of the Higher Education Commission, Thailand, for supporting him with a grant under the program Strategic Scholarships for Frontier Research Network for the Ph.D. Program Thai Doctoral degree and the Graduate School of Kasetsart University for his research. F.V. thanks the Spanish *MINECO* for postdoctoral contracts under the *Juan de la Cierva* (JCI-2010-06372) and *Ramón y Cajal* (RYC-2012-10129) programs, and F.I. acknowledges additional support through the ICREA Academia award for excellence in research. This work was also supported in part by the Air Force Office of Scientific Research under grant number FA9550-11-1-0078.

References

1 S. H. Joo, S. J. Choi, I. Oh, J. Kwak, Z. Liu, O. Terasaki and R. Ryoo, *Nature*, 2001, **412**, 169.
2 L. Gao, W. Ren, H. Xu, L. Jin, Z. Wang, T. Ma, L.-P. Ma, Z. Zhang, Q. Fu, L.-M. Peng, X. Bao and H.-M. Cheng, *Nat. Commun.*, 2012, **3**, 669.
3 M. D. Argyle and C. H. Bartholomew, *Catalysts*, 2015, **5**, 145.
4 C. Chie, Y. Chen, M.H. Engelhard and C. Song, *ACS Catal.*, 2012, **2**, 1127.
5 Y. Dai, B. Lim, Y. Yang, C. M. Cobley, W. Li, E.C. Cho, B. Grayson, P. T. Fanson, C. T. Campbell, Y. Sun and Y. Xia, *Angew. Chem. Int. Ed.*, 2010, **49**, 8165.
6 C. W. A. Chan, A. H. Mahadi, M. M.-J. Li, E. C. Corbos, C. Tang, G. Jones, W. C. H. Kuo, J. Cookson, C. M. Brown, P. T. Bishop and S. C. E. Tsang, *Nat. Commun.*, 2014, **5**, 5787.
7 B. Yang, R. Burch, C. Hardacre, G. Headdock and P. Hu, *J. Catal.*, 2013, **305**, 264.
8 D. Teschner, J. Borsodi, A. Wootsch, Z. Révay, M. Hävecker, A. Knop-Gericke, S. D. Jackson and R. Schlögl, *Science*, 2008, **320**, 86.
9 S. Vajda, M. J. Pellin, J. P. Greeley, C. L. Marshall, L. A. Curtiss, G. A. Ballentine, J. W. Elam, S. Catillon-Mucherie, P. C. Redfern, F. Mehmood and P. Zapol, *Nat. Mater.*, 2009, **8**, 213.
10 W. Gao, Z. He, Y. Qian, J. Zhao and Y. Huang, *Chem. Sci.*, 2012, **3**, 883.
11 J. Xu and M. Saeys, *J. Catal.*, 2006, **242**, 217.
12 A. Rinaldi, J.-P. Tessonnier, M. E. Schuster, R. Blume, F. Girgsdies, Q. Zhang, T. Jacob, S. B. Abd Hamid, D. S. Su and R. Schlögl, *Angew. Chem. Int. Ed.*, 2011, **50**, 3313.
13 S. M. Kozlov, I. V. Yudanov, H. A. Aleksandrov and N. Rösch, *Phys. Chem. Chem. Phys.*, 2009, **11**, 10955.
14 M. Maciejewski and A. Baiker, *Pure Appl. Chem.*, 1995, **67**, 1879.
15 M. Jiao, K. Li, W. Guan, Y. Wang, Z. Wu, A. Page and K. Morokuma, *Sci. Rep.*, 2015, **5**, 12091.
16 R. Zan, Q. M. Ramasse, U. Bangert and K. S. Novoselov, *Nano Lett.*, 2012, **12**, 3936.
17 J. Stachurski and A. Frąckiewicz, *J. Less-Common Met.*, 1985, **108**, 249.
18 J. Xu and M. Saeys, *J. Phys. Chem. C*, 2006, **242**, 217.
19 H. A. Aleksandrov, F. Viñes, W. Ludwig, S. Schauermann and K. M. Neyman, *Chem. Eur. J.*, 2013, **19**, 1335.
20 H. A. Aleksandrov, S. M. Kozlov, S. Schauermann, G. N. Vayssilov and K. M. Neyman, *Angew. Chem. Int. Ed.*, 2014, **53**, 13371.
21 A. E. Morgan and G. A. Somorjai, *Surf. Sci.*, 1968, **12**, 405-425.
22 J. Sun, Y. Nam, N. Lindvall, M. T. Cole, K. B. K. Teo, Y. W. Park and A. Yurgens, *Appl. Phys. Lett.*, 2014, **104**, 152107.
23 J. Ping and M.S. Fuhrer, *J. Appl. Phys.*, 2014, **116**, 044303.
24 H. Zi-pu, D. F. Ogeltree, M. A. van Hove and G. A. Somorjai, *Surf. Sci.*, 1987, **180**, 433.
25 T. A. Land, T. Michely, R. J. Behm, J. C. Hemminger and G. Comsa, *J. Chem. Phys.*, 1992, **97**, 6774.
26 F. Viñes, K. M. Neyman and A. Görling, *J. Phys. Chem. A*, 2009, **113**, 11963.
27 R. H. Siller, W. A. Oates and R. B. McLellan, *J. Less-Common Met.*, 1968, **16**, 71.
28 B. Longson and A. W. Thorley, *J. Appl. Chem.*, 1970, **20**, 372.
29 M. A. Quiroga, *Appl. Surf. Sci.*, 2013, **268**, 11.
30 G. Kresse and J. Furthmüller, *Comput. Mater. Sci.*, 1996, **6**, 15.
31 J. P. Perdew and Y. Wang, *Phys. Rev. B*, 1992, **45**, 13244.
32 J. P. Perdew, K. Burke and M. Ernzerhof, *Phys. Rev. Lett.*, 1996, **77**, 3865.
33 B. Hammer, L. B. Hansen and J. K. Nørskov, *Phys. Rev. B*, 1999, **59**, 7413.
34 S. H. Vosko, L. Wilk and M. Nusair, *Can. J. Phys.*, 1980, **58**, 1200.
35 D. M. Ceperley and B. J. Alder, *Phys. Rev. Lett.*, 1980, **45**, 566.
36 P. Janthon, S. M. Kozlov, F. Viñes, J. Limtrakul and F. Illas, *J. Chem. Theory Comput.*, 2013, **9**, 1631.
37 P. Janthon, S. Luo, S. M. Kozlov, F. Viñes, J. Limtrakul, D. G. Truhlar and F. Illas, *J. Chem. Theory Comput.*, 2014, **10**, 3832.
38 P. E. Blöchl, *Phys. Rev. B*, 1994, **50**, 17953.
39 A. Roldán, F. Viñes, F. Illas, J. Ricart and K. M. Neyman, *Theor. Chem. Accounts*, 2008, **120**, 565.
40 S.-G. Wang, X.-Y. Liao, D.-B. Cao, Y.-W. Li, J. Wang and H. Jiao, *J. Phys. Chem. C*, 2007, **111**, 10894.
41 F. Viñes, C. Loschen, F. Illas and K. M. Neyman, *J. Catal.*, 2009, **266**, 59.
42 F. Cinquini, F. Delbecq and P. Sautet, *Phys. Chem. Chem. Phys.*, 2009, **11**, 11546.
43 J. Gao, Q. Yuan, H. Hu, J. Zhao, and F. Ding, *J. Phys. Chem. C*, 2011, **115**, 17695.
44 D. Cheng, G. Barcaro, J.-C. Charlier, M. Hou and A. Fortunelli, *J. Phys. Chem. C*, 2011, **115**, 10537.

45 L. Nykänen, J. Andersin and K. Honkala, *Phys. Rev. B*, 2010, **81**, 075417.
46 S. B. Ziemecki, G. A. Jones, D. G. Swartzfager, R. L. Harlow and J. Faber, *J. Amer. Chem. Soc.*, 1985, **107**, 4547.
47 L. Gracia, M. Calatayud, J. Andrés, C. Minot and M. Salmeron, *Phys. Rev. B*, 2005, **71**, 033407.
48 A. Notario-Estévez, S. M. Kozlov, F. Viñes and F. Illas, *Chem. Commun.*, 2015, **51**, 5602.
49 A. Michaelides and P. Hu, *J. Chem. Phys.*, 2001, **114**, 5792.
50 J.N. Brønsted, *Chem. Rev.*, 1928, **5**, 231.
51 M. G. Evans, *Trans. Faraday Soc.* 1938, **34**, 11.
52 J. L. C. Fajín, F. Viñes, M. N. D. S. Cordeiro, F. Illas and J. R. B. Gomes, *J. Chem. Theory Comput.*, 2016, **12**, 2121.
53 A. Wiltner, C. Linsmeier and T. Jacob, *J. Chem. Phys.*, 2008, **129**, 084704.
54 T. A. Massaro and E. E. Petersen, *J. Appl. Phys.*, 1971, **42**, 5534.
55 B. S. Berry, *J. Appl. Phys.*, 1973, **44**, 3792.
56 D. J. Siegel and J. C. Hamilton, *Phys. Rev. B*, 2003, **68**, 094105.
57 S. M. Kozlov and K. M. Neyman, *J. Catal.*, 2016, **337**, 111.
58 D. Basaran, H. A. Aleksandrov, Z.-X. Chen, Z.-J. Zhao, N. Rösch, *J. Mol. Catal. A* 2011, **344**, 37.
59 H. Yokoyama, H. Numakura and M. Koiwa, *Acta Materialia*, 1998, **46**, 2823.
60 H. Gabasch, K. Hayek, B. Klotzer, A. Knop-Gericke and R. Schlögl, *J. Phys. Chem. B*, 2006, **110**, 4947.
61 F. Viñes, Y. Lykhach, T. Staudt, M. P. A. Lorenz, C. Papp, H.-P. Steinrück, J. Libuda, K. M. Neyman and A. Görling, *Chem. Eur. J.*, 2010, **16**, 6530.
62 S. Schauermann, J. Hoffmann, V. Johánek, J. Hartmann, J. Libuda and H.-J. Freund, *Angew. Chem. Int. Ed.*, 2002, **41**, 2532.
63 K. M. Neyman and S. Schauermann, *Angew. Chem. Int. Ed.*, 2010, **49**, 4743.
64 V. P. Babar, S. Jaiswal and V. Kumar, *Chem. Phys. Lett.*, 2013, **560**, 42.
65 F. Viñes, J. R. B. Gomes and F. Illas, *Chem. Soc. Rev.*, 2014, **43**, 4922.
66 F. Calle-Vallejo, J. Tymoczko, V. Colic, Q. H. Vu, M. D. Pohl, K. Morgenstern, D. Loffreda, P. Sautet, W. Schuhmann and A. S. Bandarenka, *Science* 2015, **350**, 185.
67 M. Shao, Q, Wang, J.-P. Dodelet and R. Chenitz, *Chem. Rev.*, 2016, **116**, 3594.
68 M. Ahmadi, C. Cui, H. Mistry, P. Strasser and B. R. Cuenya, *ACS Nano*, 2015, **9**, 10686.
69 S. L. Knupp, M. B. Vukmirovc, P. Haldar, J. A. Herron, M. Mavrikakis and R. R. Adzic, *Electrocatal.*, 2010, **1**, 213.
70 Z. Gu and P. B. Balbuena, *J. Phys. Chem. C*, 2007, **111**, 9877.